Eur. J. Phys. 16 (1995) 275–281. Printed in the UK

The one-dimensional bubble: An unusual oscillator, with applications to human bioeffects of underwater sound

T G Leighton, P R White, M A Marsden

Institute of Sound and Vibration Research, University of Southampton, SO17 1BH, UK

Received 4 May 1995, in final form 4 July 1995

Abstract. In this paper the oscillation dynamics of a linear gas pocket in a liquid are analysed. These include several features of potential use at undergraduate level for illustrating characteristics beyond those normally encountered in expositions of simple harmonic oscillators. The oscillator in question is unusual first in that, as with all gas bubbles in liquid, the inertia is invested primarily in the surrounding liquid, rather than in the pocket itself. Second, a nonlinearity arises through the displacement dependence of the oscillator stiffness. These effects are included in the equation of motion of a damped, forced, one-dimensional bubble, which is solved numerically. Analytical solutions for the natural frequency of small-amplitude undamped oscillations in the linear limit are also obtained, and both are compared with experimental measurements of the phase and amplitude response of a laboratory one-dimensional bubble. The analysis is used to indicate the response of air bubbles within the ear canals of divers to low frequency underwater sound, and the potential of bubbles in lung blood vessels to cause haemorrhage when subjected to lithotripsy.

Abstrakt. In dieser Arbeit werden Schwingungsbewegungen von zylindrischen Gaseinschluessen in Flüssigkeiten untersucht. Dies beinhaltet Möglichkeiten zur populärwissenschaftlichen Darstellung von harmonischen Schwingern über das bisher Übliche hinaus. Wie alle Gasbläschen in Flüssigkeiten ist der hier untersuchte Schwinger in erster Linie deshalb so ungewöhnlich, weil seine träge Masse ohne Umhüllung von der umgebenden Flüssigkeit eingeschlossen ist. Daneben führt die von der Auslenkung abhängige Steife des Schwingers zu einem nichtlinearen Verhalten. Diese Effekte gehen in die numerisch zu lösende Bewegungsgleichung einer gedämpften, erzwungenen Schwingung eindimensionaler Bläschen ein. Diese und analytische Lösungen für die Eigenfrequenz von ungedämpften, linearen Schwingern werden mit dem unter Laborbedingungen experimentell ermittelten Amplituden- und Phasenverhalten von eindimensionalen Gasbläschen verglichen. Mit Hilfe dieser Analyse werden Rückschlüsse auf das Verhalten von Luftbläschen im Ohrkanal von Tauchern bei tieffrequentem Unterwasserschall als auch auf die bei einer Lithotripsie vorhandene Blutungsgefahr durch Gasbläschen in Lungenblutge-fäßen gezogen.

1. Introduction

Most students are introduced to the physics of oscillators through the behaviour of an idealized mass-spring system. If the bob of mass m undergoes a displacement ϵ, the spring (assumed to be massless) responds by applying a force $-k\epsilon$. Therefore, from Newton's third law, the spring constant k can be defined from the ratio of the applied force F required to produce a displacement ϵ to that displacement, or more generally:

$$k = \frac{\mathrm{d}F}{\mathrm{d}\epsilon} \tag{1}$$

If there is a damping force proportional to the speed of the bob, then the equation governing the motion of the bob is found from Newton's second law to be

$$m\ddot{\epsilon} + b\dot{\epsilon} + k\epsilon = F \tag{2}$$

where F represents any external forces applied to drive the system. In the absence of a driving force and damping, substitution of the linear solution $\epsilon = \epsilon_0 \cos \omega_0 t$ into equation (2) shows that the disturbed system undergoes oscillation at the natural circular frequency ω_0,

0143-0807/95/060275+07$19.50

where

$$\omega_0 = \sqrt{\frac{k}{m}} \tag{3}$$

which is independent of ϵ_0, the amplitude of the displacement. Equation (3) can also be obtained by equating the maximum kinetic energy of the system, $\Phi_{K,\max}$, which is attained when the bob passes through the equilibrium position ($\epsilon = 0$; $|\dot{\epsilon}| = \omega_0\epsilon_0$), with the maximum potential energy that is stored in the system, $\Phi_{P,\max}$. The potential energy stored in the spring reaches a maximum at either extreme of the motion ($\epsilon = \epsilon_0$; $|\dot{\epsilon}| = 0$) such that

$$\Phi_{P,\max} = \int_0^{\epsilon_0} k\epsilon \, d\epsilon = \tfrac{1}{2}k\epsilon_0^2. \tag{4}$$

Equating this to

$$\Phi_{K,\max} = \tfrac{1}{2}m|\dot{\epsilon}_{\max}|^2 = \tfrac{1}{2}m(\omega_0\epsilon_0)^2 \tag{5}$$

yields equation (3), the natural frequency of the undamped oscillator, which damping will tend to reduce (French, 1979). This idealized system is sufficient to illustrate how the ratio of the two primary characteristics of the oscillator, stiffness and inertia (represented above by k and m respectively) relate to the natural frequency for undamped motion. The preceding idealized model differs from the real spring/bob oscillator in both the stiffness and inertia. The stiffness is independent of the displacement only at small amplitudes: The spring may be extended beyond its elastic limit, and the motion becomes history-dependent. Whilst the inertia in the simple model is invested wholly in the bob, acceleration of a real bob causes accelerations in the spring, increasing the system inertia. However when the bob is displaced upwards, a volume of air must be displaced downwards: the driver must provide not only the kinetic energy of the bob and the spring but also the kinetic energy of an amount of the surrounding gas. The inertial contribution from the surrounding fluid is characterized by the so-called 'radiation mass' m_r, which is defined through $\Phi_{KE,\max}$, the maximum kinetic energy of the surrounding *fluid* only, in the following way:

$$\Phi_{KE,\max} = \tfrac{1}{2}m_r|\dot{\epsilon}_{\max}|^2 = \tfrac{1}{2}m_r(\omega_0\epsilon_0)^2 \tag{6}$$

These departures from the ideal spring-bob oscillator are accentuated in bubbles. Whilst in the spring/bob oscillator the radiation mass is generally negligible in comparison with the bob inertia, when gas is trapped in bubbles in liquid, the inertia associated with acceleration of the relatively dense liquid is very much greater than the inertia of the gas itself. It will also be shown that the stiffness of the one-dimensional bubble is dependent on the displacement. Whilst the nonlinear oscillations of three-dimensional bubbles have been studied for some time (Leighton, 1994), less is known of one-dimensional bubbles, which may feature significantly

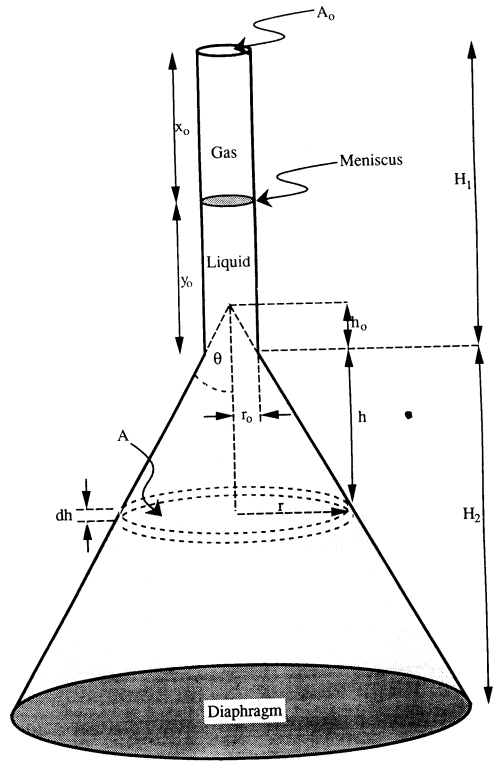

Figure 1. Schematic of 1-D bubble.

in the interaction with sound of gas pockets within several biological structures.

The natural frequency of the undamped one dimensional bubble can be calculated by equating the maximum potential energy with the maximum kinetic energy, as was done for the idealized spring/bob model in equations (3) to (5). The idealized one-dimensional bubble analysed here and shown in figure 1, is modelled as a cylindrical pocket of gas contained within rigid walls except at the flat interface with the liquid, which can move only in a piston-like manner. The liquid is contained within the rigid walls of a connected tube and cone. The liquid is assumed to be incompressible, and all the potential energy is taken to be invested within the compressibility of the gas. Assume that the gas within the bubble behaves polytropically, such that

$$pV^{\kappa} = \text{constant} \tag{7}$$

where p is the gas pressure within the bubble, of volume V, and where κ is the so-called polytropic index (which varies between γ, the ratio of the specific heat of the gas at constant pressure to that at constant volume, and unity, depending on whether the gas is behaving adiabatically, isothermally, or in some intermediate manner). If an incremental meniscus displacement $d\epsilon$ occurs, and the bubble volume changes by $dV = A_0\,d\epsilon$, then integration of the incremental change in the potential energy,

$d\Phi_{PE} = -(p - p_0)\,dV$, from equilibrium to the extreme of the oscillation, gives the maximum potential energy stored in the gas to be:

$$\Phi_{PE,max} = \int_0^{\epsilon_0} \frac{\kappa A_0 p_0}{x_0}\epsilon\,d\epsilon = \left(\frac{\kappa A_0 p_0}{x_0}\right)\frac{\epsilon_0^2}{2}. \quad (8)$$

If the inertia of the gas is assumed to be negligible, and the liquid meniscus undergoes a harmonic displacement ϵ, then the maximum meniscus speed $|\dot{\epsilon}_{max}| = \omega_0\epsilon_0$ occurs when $\epsilon = 0$. The maximum kinetic energy of the liquid is found by integrating the contributions from parallel elements of infinitesimal vertical thickness dh when $\epsilon = 0$, noting how since the cross-sectional area in the cone increases with distance from the meniscus, the flow velocity of the incompressible liquid decreases in proportion:

$$\Phi_{KE,max} = \tfrac{1}{2}\rho A_0 y_0 \omega_0^2 \epsilon_0^2 + \int_{h_0}^{H_2}\left(\tfrac{1}{2}\rho\pi(h\tan\theta)^2|\dot{\epsilon}_{max}|^2\left(\frac{A_0}{\pi(h\tan\theta)^2}\right)^2\right)dh$$

$$= \frac{1}{2}\left[\rho A_0 y_0 + \frac{\rho A_0^2}{\pi\tan^2\theta}\left(\frac{1}{h_0} - \frac{1}{H_2}\right)\right](\epsilon_0\omega_0)^2 \quad (9)$$

Comparison of equations (9) and (6) shows that the radiation mass m_r equals the expression in square brackets. It comprises two terms: the first, $\rho A_0 y_0$, is the mass of liquid in the column; and the second corresponds to the inertia of the liquid in the cone. The natural frequency of the undamped oscillator is found, as before, by equating $\Phi_{KE,max}$ to $\Phi_{PE,max}$, which can be done through equations (8) and (9) to give

$$\omega_0 = \sqrt{\frac{\kappa p_0}{\rho z_0\left((H_1 - x_0)(1 + \Lambda/r_0)\dfrac{A_0}{\pi\tan^2\theta}\left(\dfrac{1}{h_0} - \dfrac{1}{H_2}\right)\right)}} \quad (10)$$

where liquids of finite viscosity μ require the factor $(1 + \Lambda/r_0)$, r_0 being the radius of the cylinder and $\Lambda = \sqrt{2\mu/\rho\omega_0}$ being the viscous boundary layer thickness (Miller and Nyborg, 1983).

Since m_r is now known, comparing equations (10) and (3) yields the stiffness under the assumption of oscillations of infinitesimal amplitude to be $\kappa p_0 A_0/x_0$. At finite amplitude, the stiffness can be found through application of equation (7) to equation (1) (Leighton *et al* 1995):

$$k = A_0\frac{\partial p}{\partial\epsilon} = \frac{\kappa p_0 A_0^2}{V_0}\left(1 - \frac{A_0\epsilon}{V_0}\right)^{-(\kappa+1)} \quad (11)$$

These two components, inertia (m_r) and stiffness (k) can therefore be incorporated into the equation of motion which, with an appropriate damping term (b), resembles equation (2):

$$m_r\ddot{\epsilon} + b\dot{\epsilon} + k\epsilon = F \rightarrow \left(\rho A_0 y_0\left((1 + \Lambda/r_0) + \frac{A_0}{y_0\pi\tan^2\theta}\left(\frac{1}{h_0} - \frac{1}{H_2}\right)\right)\right)\ddot{\epsilon} + b\dot{\epsilon} + \frac{\kappa p_0 A_0^2}{V_0}\left(1 - \frac{A_0\epsilon}{V_0}\right)^{-(\kappa+1)}\epsilon = F \quad (12)$$

The analytical treatment of the equations of motion which are damped, forced, or both, is not feasible. The solution to equation (12) requires the adoption of the numerical path, and here standard Runge-Kutta algorithms are used (Forsythe *et al* 1977). A sinusoidal form for the forcing term is assumed. The size of the damping term can be obtained from theory, and has been solved for similar geometries, though the analysis is not simple (Miller and Nyborg 1983, Miller and Neppiras 1985). For comparison of theory and experiment, the quality factor was measured from the width of the resonance in the data plots (figures 3 and 4), and a typical value ($Q = 3.5$) was incorporated into solutions of equation (12).

2. Experimental

A laboratory one-dimensional model bubble was constructed to verify this theory. It comprises glass capillary tubing of ≈ 123 mm length (with 1.5 mm internal diameter and 2 mm wall thickness), attached to an inverted glass funnel ($\theta = 30°$, $H_2 = 43.3$ mm). A rubber diaphragm, bolted to a vibrator, covers

Figure 2. The apparatus employed to measure the phase response of a driven bubble.

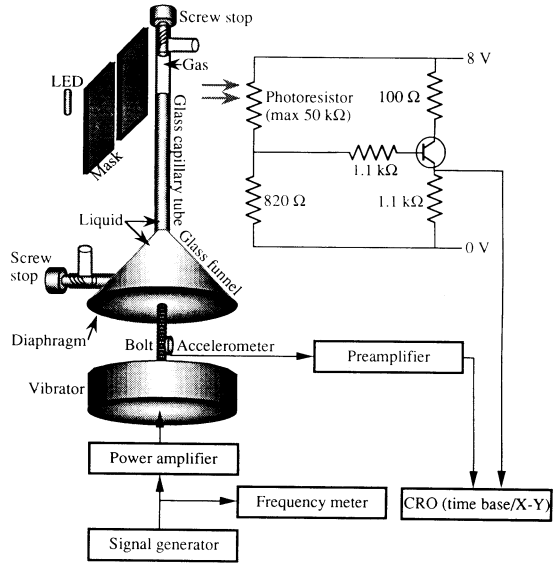

the funnel base (figure 2). The area ratio of the funnel mouth to the capillary produces a meniscus displacement approximately twenty times greater than the diaphragm displacement, facilitating meniscus observation and minimizing glassware vibration. The glassware has two stopcocks attached at either end of the capillary to enable both the control of pressure and the introduction of a known amount of liquid (which was degassed, filtered, and coloured with food dye). A sinewave generator (Therlby Thandor TG220) and amplifier drive the vibrator (Ling 409), the acceleration of which is measured via accelerometer and charge amplifier (Bruel and Kjaer 4367 and 2635 respectively) using a storage oscilloscope (Gould OS1420).

Two types of measurements were made, each requiring a different set of equipment. The phase sensor comprised a photoresistor (NORP-12) and an LED, masked to minimize all but direct path light transmission: Obscuration of the light by the dyed water produced a signal which could be used to monitor the meniscus displacement (figure 2), the driver (accelerometer signal) and response (photoresistor) signals being displaced as an $X - Y$ plot to determine their phase relationship, duly compensating for phase response of the electronics. The light detector signal was low-pass filtered (Barr and Stroud type EF3-04 set to 50 Hz), reducing mains interference. A 40 Hz low-pass filter (Fern Developments type EF5-02) reduced noise in the accelerometer signal.

The *phase* response was found for constant driver acceleration amplitude. To achieve this constancy, the input voltage was reduced as the frequency was increased. This decreases the meniscus *displacement* to near-invisibility, so that in measuring the amplitude resonance the driver input voltage was kept constant as the frequency, and therefore the vibrator acceleration, increased. The meniscus displacement amplitude was measured by travelling microscope (Type 2162-HB) with stroboscopic (Dawe type 1204C) illumination at approximately twice the driver frequency.

3. Results

The experimental results, taken at discrete frequencies, demonstrate the phase relationship between the driver and one bubble (figure 3), and the amplitude response of another bubble (figure 4), as a function of frequency. Table 1 summarizes the experimental parameters and resonance frequencies, as determined from these experimental data, and as calculated (for $\kappa = 1$ and $\kappa = \gamma$) from small-amplitude linear theory (equation (10), and through integration of equation (12). The results of these integrations, which allow for finite amplitude nonlinear damped oscillations and employ the experimentally-determined quality factor of 3.5, are shown in figures 3 and 4 as

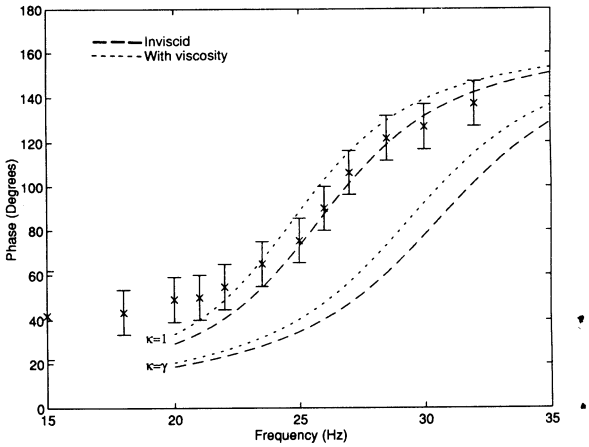

Figure 3. The phase response of a driven air bubble in water ($x_0 = 71.5 \pm 0.5$ mm, $y_0 = 52.0 \pm 0.5$ mm). Vibrator acceleration amplitude: 8.92 m s^{-2}. Experimental measurements at discrete frequencies are shown. The numerical solutions are shown for the adiabatic ($\kappa = \gamma$) and isothermal ($\kappa = 1$) cases, as the labels show. Solutions to the equation of motion (equation (12)) are shown for both cases of water with finite viscosity (short dashed line - - - - - labelled 'with viscosity) and with zero viscosity (long dashed line – – – –, labelled 'inviscid').

Figure 4. The amplitude response of an air bubble in water ($x_0 = 70.0 \pm 0.5$ mm, $y_0 = 53.0 \pm 0.5$ mm), driven with a vibrator acceleration amplitude which increases linearly with frequency from 9 m s^{-2} at 15 Hz to 45 m s^{-2} at 36 Hz. Experimental measurements at discrete frequencies are shown. The numerical solutions are shown for the adiabatic ($\kappa = \gamma$) and isothermal ($\kappa = 1$) cases, as the labels show. Solutions to the equation of motion (equation (12)) are shown for both cases of water with finite viscosity (short dashed line - - - - - labelled 'with viscosity') and with zero viscosity (long dashed line – – – –, labelled 'inviscid').

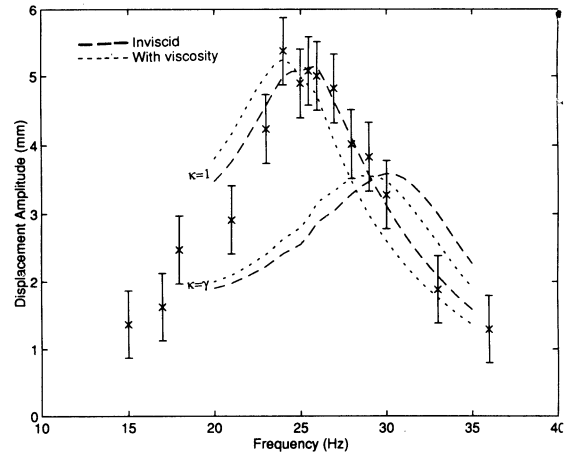

Table 1. Comparison of the experimentally determined resonances with those determined by theory: linear (equation (10)) and numerical (equation (12)), for $p_0 = 10^5$ Pa, $\mu = 10^{-3}$ Pa s and $\rho = 1000\,\mathrm{kg\,m^{-3}}$. Bubble size and vibrator acceleration are indicated.

Fig	x_0 mm	y_0 mm	Vibrator acceleration amplitude (s^{-2} m)	Resonance (Linear theory, (10)) (Hz)	Resonance (Numerical theory, (12)) (Hz)	Resonance (Experimental) (Hz)
3	71.5 ± 0.5	52.0 ± 0.5	8.92	24.1 ± 0.2 ($\kappa = 1$) 28.8 ± 0.2 ($\kappa = 1.4$)	25.0 ± 0.5 ($\kappa = 1$) 30.0 ± 0.5 ($\kappa = 1.4$)	26 ± 1
4	70.0 ± 0.5	53.0 ± 0.5	See caption to figure 4	24.4 ± 0.2 ($\kappa = 1$) 28.8 ± 0.2 ($\kappa = 1.4$)	24.0 ± 0.5 ($\kappa = 1$) 29 ± 1 ($\kappa = 1.4$)	26 ± 2

dotted plots for $\kappa = 1$ and $\kappa = \gamma$, (labelled 'with viscosity'). To demonstrate the importance of viscosity (an effect which is often of secondary importance for spherical bubbles—Minnaert, 1933), dashed lines (labelled 'inviscid') in figures 3 and 4 show the result of setting μ to zero in equation (12).

4. Discussion

A gas which is assumed to behave polytropically, as this is, should give data points which lie *between* the extremes given the relevant $\kappa = 1$ and $\kappa = \gamma$ curves in the results. The tendency in figure 3 is for the data to fall between the 'with viscosity' curves (except at the lowest frequencies). Taking the viscous theory therefore to more accurately model the process, of the two extremes ($\kappa = 1$ and $\kappa = \gamma$) the data points are closer to the isothermal line, indicating that κ is just greater than 1. Figure 3 therefore suggests that one would expect, for a given point on the resonance curve (e.g. a certain phase in figure 3, or a pre- or post-maximum condition on the amplitude plot), each data point would lie at a slightly higher frequency than that predicted by an isothermal theory which incorporates viscosity. This is indeed what is seen on the amplitude plot (figure 4). The value of Λ for the experimental bubble investigated here is around 10^{-4} m, such that the $\sqrt{(1 + \Lambda/r_0)}$ correction factor in the denominator of equation (10) causes an 8% frequency reduction. This is significantly larger than the 0.5% reduction which results from using the radiation mass, rather than the mass of liquid in the column, $\rho A_0 y_0$, for the inertia.

The dynamics of similar oscillators have been studied in the past. Howkins (1965) made observations and preliminary calculations regarding the oscillations of gas bubbles in water attached to the submerged base of an inverted vibrator (both roughly spherical bubbles beneath a plane face, and gas pockets trapped within 'pits' within the base). A cylindrical micron-sized bubble bounded by elastic walls (such as occurs between plant cells within *Elodea*, where the stiffness of the plant wall can be dominant over the stiffness of the gas) may vibrate in the radial mode, the motion of the end-walls being less important (Miller 1977, 1979). Even if the walls are rigid, other motions can occur beyond the piston-like oscillation of the meniscus as it undergoes a Bessel-function deformation, the so-called 'clamped-drumhead' vibration (Miller 1979, Miller and Nyborg 1983, Miller and Neppiras 1985).

Biological structures may contain one-dimensional bubbles, and two examples of these in particular are exposed to intense sound. The first case is of one-dimensional bubbles trapped within ear canals of divers, and the adverse effects on divers and other mammals exposed to high intensity sound in the marine environment is currently of great concern. The second case is of one-dimensional bubbles trapped within capillary blood vessels. This may occur particularly in the lung, and evidence suggests that the lowest thresholds for damage by clinical ultrasound in mammals *in vivo* are found in the lung.

Divers today are increasingly exposed to high-intensity sound in the underwater environment. Tools used in underwater construction may produce sound pressure levels (SPL) as large as 210 dB SPL (re 20 μPa) (Molvaer and Gjestland 1981, Nedwell *et al* 1993) over a wide range of frequencies. Other emissions result from techniques associated with communication, exploration, monitoring, and exploitation of the oceans by man. Of particular interest recently are experiments involving the propagation of low frequency sound (from a few tens of hertz up to around 250 Hz) over long ranges (of order 1000 km) for climate monitoring, using powerful sources (e.g. 220 dB re 1 μPa at 1 m—Baggeroer and Munk 1992).

Air bubbles may be trapped within diver ear canals, and can significantly affect underwater hearing (Al Masri 1993). A cylindrical bubble is visualized, bounded by the curved canal walls, the ends being at the ear drum and the gas/water interface within the ear canal. The remainder of the canal would be water-filled leading to the pinna, and thence to the water surrounding the head. The

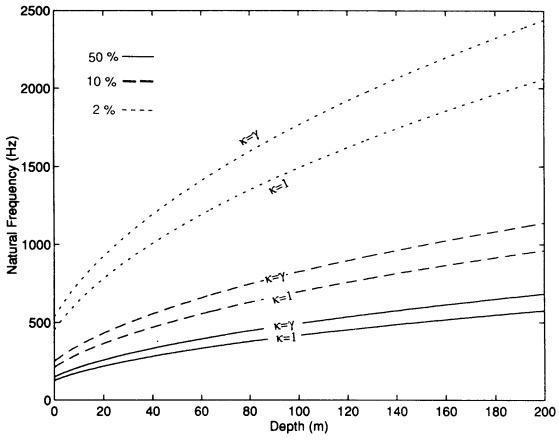

Figure 5. Resonance of air bubbles in ear canals as a function of ambient pressure (or equivalently, depth) for typical ear canal (2.5 cm long, having 5 mm diameter—Davis 1978) filled to (a) 50% (solid line ——), and (b) 10% (long dashed line – – – –) and (c) 2% (short dashed line - - - - -) operating in a piston-like manner. Viscosity is incorporated ($\mu = 10^{-3}$ Pa s), but the inertia of the liquid outside the canal is neglected (justified since the filling of air is to less than 50%). This is an extrapolation of the theory. Acceleration due to gravity = 9.8 m s^{-2}.

fleshy boundaries, though elastic, will for these estimations be assumed to be rigid. As in this experiment, the inertia will be invested primarily in the water column, assuming this fills the canal to at least 50%. The radiation mass of the water outside the head is less significant, and the inertia of the entrained gas is negligible. Given typical ear canal dimensions (figure 5), extrapolation of simple linear theory predicts that air bubbles trapped within divers' ears may be expected to resonate at frequencies which may occur at high intensity in the underwater environment.

Such resonances, and their harmonics, clearly may cause a noticeable effect within a system designed to be sensitive to acoustic stimulation through gas, rather than liquid, adjacent to the eardrum. The mechanisms of underwater hearing are involved, and it is not a simple matter to extrapolate how bubbles may affect divers. However human diving is potentially hazardous, and the occurrence of any reasonances coupling the human hearing, orientation and balance systems to an ocean medium which can contain intense sound at those frequencies must be considered.

'Gas body activation' (Miller 1984), the ultrasonic excitation of gas pockets stabilized within biological structures such as plant vessels, blood vessels, insect trachae and mammalian cells, is more documented. There exists a range of mechanisms, both cavitational and non-cavitational mechanisms, through which ultrasound may generate a bioeffect (ter Haar 1986). Whilst 'stable' cavitation, where 'spherical' bubbles pulsate over many cycles, may generate bioeffects (Vivino 1985), damage is more often associated with 'transient' cavitation, where the bubble grows explosively to then collapse, generating high-amplitude pressure fluctuations in the gas and the liquid (Leighton 1994). High-intensity microsecond lithotripsy pulses can clearly affect bubbles, and the most sensitive organ to such exposure is the lung. Fetal murine lung has a lower threshold for damage than adult lung has (Hartman 1990), presumably because of the absence of stabilised gas bodies within the fetal lung (ter Haar *et al* 1994). Noting that Child *et al* (1990) and Frizzell *et al* (1994) have observed haemorrhage in mammalian lung resulting from exposure to pulsed ultrasound at low levels compared to those required to produce cavitation in tissues that do not contain stabilized gas bodies, ter Haar *et al* (1994) comment that whilst the mechanism is not clear, it does appear to be mediated by existing stabilized gas bodies in tissue.

Differences exist between mechanisms based on spherical bubbles, and on one-dimensional stabilized bubbles. Both bubble types may undertake 'stable' and 'transient' behaviour. However in the latter it may be the *growth* phase, not (as with spherical bubbles) the collapse, which may cause bioeffect. If a biological structure resists the growth of a bubble it encapsulates, it may be damaged by the resulting stresses (Ward *et al* 1983, Venter *et al* 1983, Aymé and Carstensen 1989). The hypothesis to be examined here is that bubbles need not be encapsulated by structure for damage during growth to happen if, like one-dimensional bubbles within lung capillaries, they are within a tube-like structure. Such cylindrical gas pockets might arise through (i) the ultrasonically-induced growth of a tiny nucleus to fill the vessel cross-section; (ii) the migration of a gas body through the branching arteries until it eventually lodges in a small vessel of similar diameter to its own. Such gas bodies may originate through echo-contrast agents, or simple exsolution, since conditions within the blood flowing from heart to lung are designed to encourage gas to come out of solution. Once the geometry of the one-dimensional bubble is attained, the liquid inertia controls the ultrasonically-induced growth.

This response of the one-dimensional bubble from this moment becomes radically different from that of the free-floating spherical bubbles, since the inertial term does not asymptotically tend to a finite value. A pulsating spherical bubble, of equilibrium and instantaneous radii R_0 and R respectively, has a radiation mass of value $4\pi R_0^3 \rho$ (Leighton 1994), a finite and relatively small value because the spherically diverging geometry causes the liquid particle velocity $\dot{r}$ at a distance r from the bubble centre to follow an inverse-square law, $\dot{r} = \dot{R}(R^2/r^2)$ (Minnaert 1933), such that $\dot{r} \to 0$ as $r \to \infty$. Therefore the total kinetic energy of the liquid is finite, even within an infinite liquid medium. In contrast

the liquid geometry in the one-dimensional bubble system shown in figure 1 does not diverge until the cone section, the inertial contribution from the liquid contained within the glass capillary tube increasing monotonically with the tube length (as can be seen from equation (9): the inertia of the liquid in the pipe is $\rho A_0 y_0$). In contrast to the spherical case, a one-dimensional bubble within an infinite non-diverging pipe would have infinite inertia, and so is not an oscillator. Therefore in the blood circulatory system, where the geometry does not simply and rapidly diverge but consists of long branching tubes, the inertia of such a bubble would be very high. Rebounding after the passage of a compressive pulse or under a tension, the bubble cannot move the massive column of liquid, and the stress will be exerted to the capillary wall and the meniscus. If the stresses so exerted are greater than the cohesion between the single layer of cells of the capillary wall, then haemorrhage will occur. The only other 'give' when the one-dimensional bubble expands within the blood vessel in the meniscus: this will bow, causing local fluid motion and in the first instance, small gas volume change. For deformation extreme enough to generate daughter bubbles (which could seed further expansions), a uniformly-bowing meniscus must pass through the hemispherical condition, where the surface tension pressure is a maximum. For a typical capillary of diameter $\approx 10\,\mu$m this corresponds to a confining pressure of ≈ 23 kPa, giving a lower limit for the adhesion required to prevent haemorrhage. The ultimate tensile strength of the weakest tissue noted by Yamada (1973) is 50 kPa. In summary, the geometry acts against allowing the large-scale gas expansion required to relieve the stress on the capillary wall, and so prevent haemorrhage.

5. Conclusions

The dynamics of a one-dimensional bubble were developed, including a simple analysis of small-amplitude linear oscillations, and numerical solution to the full equation of motion. The analyses were capable of predicting resonance of laboratory bubbles of centimetre-order length. The physical insights gained by the models allowed examination of the potentially biologically-significant cases of acoustic exposure of one-dimensional bubbles in divers' ear canals and within mammalian lung capillaries.

References

Al Masri M A O 1993 Ph.D. Thesis *Underwater Hearing Thresholds and Hearing Mechanisms* University of Southampton

Aymé E J and Carstensen E L 1989 *IEEE Trans. on Ultrasonics, Ferroelectrics and Frequency Control* **36** 32–40

Baggeroer A and Munk W 1992 *Physics Today* **45** 22–30

Child S Z, Hartman C L, Schery L A and Carstensen E L 1990 *Ultrasound Med. Biol.* **16** 817

Davis H 1978 Anatomy and Physiology of the Auditory System *Hearing and Deafness* ed H Davis and S R Silverman (New York: Holt, Rinehart and Winston) 4th Edition ch 3

Devin C Jr 1959 *J. Acoust. Soc. Am.* **31** 1654

Forsythe G E, Malcom M A and Moler L B 1977 *Computer Methods for Mathematical Computations* (Englewood Cliffs, NJ: Prentice-Hall)

French A P 1979 *Vibrations and Waves* (London: Nelson)

Frizzell L A, Chen E and Lee C 1994 *Ultrasound Med. Biol.* **20** 53–63

Hartman C, Child S Z, Mayer R, Schenk E and Carstensen E L 1990 *Ultrasound Med. Biol.* **16** 675–9

Howkins S D 1965 *J. Acoust. Soc. Am.* **37** 504–8

Leighton T G 1994 *The Acoustic Bubble* (London: Academic)

Leighton T G, White P R and Marsden M A 1995 *ISVR Technical Report* No. 246

Miller D L 1977 *Ultrasound Med. Biol.* **3** 221–40

——— 1979 *J. Acoust. Soc. Am.* **65** 1313–1321

——— 1984 *Ultrasonics* **22** 261–9

Miller D L and Neppiras E A 1985 *J. Acoust. Soc. Am.* **77** 946–53

Miller D L and Nyborg W L 1983 *J. Acoust. Soc. Am.* **73** 1537–44

Minnaert M 1933 *Phil. Mag.* **16** 235–48

Molvaer O I and Gjestland T 1981 *Scan. J. Work Environ. Health* **7** 263–270

Nedwell J R, Martin A M and Mansfield N 1993 *Advances in Underwater Technology* (Deventer: Kluwer) **31** 267–75

ter Haar G R 1986 Therapeutic and surgical applications *Physical principles of Medical Ultrasonics* ed C R Hill (New York: Wiley) part III

ter Haar G, Frizzell L A, Delius M and Stratmeyer M 1994 Non-thermal bio-effects: Organs, Cells, Tissues *WFUMB Symposium on Safety of Ultrasound in Medicine: Emphasis on non-thermal mechanisms* Ch 5 (draft)

Venter R D, Ward C A, Ho S, Johnson W R, Fraser W D and Landolt J P 1983 *Undersea Biomed. Res.* **10** 225–40

Vivino A A, Boraker D K, Miller D and Nyborg W 1985 *Ultrasound in Med. & Biol.* **11** 751–9

Ward C A, Johnson W R, Venter R D, Ho S, Forest T W and Fraser W D 1983 *J. Appl. Phys.* **54** 1833–43

Yamada H 1973 *Strength of Biological Materials* ed F G Evans) (New York: Krieger)

Due to a printer's error, the following equation was incorrectly printed. The correct equation is shown below.

$$\omega_0 = \sqrt{\frac{\kappa p_0}{\rho x_0 \left(\left(H_1 - x_0 \right) \left(1 + \Lambda / r_0 \right) + \frac{A_0}{\pi \tan^2 \theta} \left(\frac{1}{h_0} - \frac{1}{H_2} \right) \right)}} \tag{10}$$